Overexpression of Sphingosine Kinase 1 Prevents Ceramide Accumulation and Ameliorates Muscle Insulin Resistance in High-Fat Diet–Fed Mice

Clinton R. Bruce,[1,2] Steve Risis,[1] Joanne R. Babb,[1] Christine Yang,[1] Greg M. Kowalski,[2] Ahrathy Selathurai,[2] Robert S. Lee-Young,[1] Jacquelyn M. Weir,[3] Kazuaki Yoshioka,[4] Yoh Takuwa,[4] Peter J. Meikle,[3] Stuart M. Pitson,[5] and Mark A. Febbraio[1]

The sphingolipids sphingosine-1-phosphate (S1P) and ceramide are important bioactive lipids with many cellular effects. Intracellular ceramide accumulation causes insulin resistance, but sphingosine kinase 1 (SphK1) prevents ceramide accumulation, in part, by promoting its metabolism into S1P. Despite this, the role of SphK1 in regulating insulin action has been largely overlooked. Transgenic (Tg) mice that overexpress SphK1 were fed a standard chow or high-fat diet (HFD) for 6 weeks before undergoing several metabolic analyses. SphK1 Tg mice fed an HFD displayed increased SphK activity in skeletal muscle, which was associated with an attenuated intramuscular ceramide accumulation compared with wild-type (WT) littermates. This was associated with a concomitant reduction in the phosphorylation of c-jun amino-terminal kinase, a serine threonine kinase associated with insulin resistance. Accordingly, skeletal muscle and whole-body insulin sensitivity were improved in SphK1 Tg, compared with WT mice, when fed an HFD. We have identified that the enzyme SphK1 is an important regulator of lipid partitioning and insulin action in skeletal muscle under conditions of increased lipid supply. ***Diabetes*** **61:3148–3155, 2012**

Obesity is associated with the development of insulin resistance and type 2 diabetes. The pathogenesis of insulin resistance is a well-investigated area, yet the precise interplay between the molecular pathways that leads to this disorder is not fully understood (1). Extensive evidence, however, suggests that defects in fatty acid (FA) metabolism and subsequent lipid accumulation in liver and skeletal muscle play a major role (2,3). Although the increase in lipid manifests as an increase in triacylglycerol (TAG), it is likely that this is a marker of dysfunctional FA metabolism and that accumulation of bioactive lipids, such as ceramide and diacylglycerol (DAG), impair insulin action. DAG accumulation in muscle is associated with insulin resistance in humans (4), whereas mice with DAG kinase delta haploinsufficiency display increased DAG content and reduced peripheral insulin sensitivity (5).

Ceramide is a potent lipid-signaling molecule that can cause insulin resistance by inhibiting the ability of insulin to activate Akt (6) and/or via the activation of c-jun amino terminal kinase (JNK) (7,8). Importantly, preventing ceramide accumulation by inhibiting de novo ceramide synthesis protects against the development of insulin resistance (9,10). These observations support the hypothesis that increases in ceramide are an important mechanism underlying the development of muscle insulin resistance, and therefore, targeting pathways to prevent ceramide accumulation may be a viable therapeutic approach.

One such approach is to increase ceramide degradation and clearance. Two important enzymes in this pathway are ceramidase and sphingosine kinase (SphK). Ceramidase is responsible for converting ceramide to sphingosine, and SphK phosphorylates sphingosine to sphingosine 1 phosphate (S1P). Because breakdown of S1P is the only way for cellular lipids to exit the sphingolipid pathway, SphK is important in regulating sphingolipid metabolism (11). SphK exists in two isoforms, SphK1 and SphK2. Despite clear evidence that SphK1 activation reduces ceramide (12,13), the role of SphK1 in regulating insulin action has been largely overlooked. Activation of SphK1 prevents ceramide accumulation by promoting its metabolism into S1P. SIP is a molecule with many complex functions: it not only activates five specific G-coupled protein receptors that subsequently activate many downstream signaling pathways but also has important second messenger actions (14). SIP is generally thought to promote activation of inhibitor of κ kinase-β (IKK-β) and JNK via upstream activation of transforming growth factor-β–activated kinase 1 (14), however, SphK1 can block JNK activation (13,15) and prevent tissue inflammation (15), which is linked to insulin resistance (16). In contrast, inhibiting SphK1 leads to JNK activation (17). Interestingly, S1P itself opposes the effects of ceramide. For example, S1P has been shown to counteract ceramide-induced activation of JNK (18). Thus, it has been proposed that the ceramide-to-S1P ratio may function as an intracellular rheostat (19,20).

Although not well studied in the context of metabolic disease, evidence is emerging to suggest that the sphingolipid rheostat is important in regulating insulin action. Adiponectin has been thought to exert insulin-sensitizing effects via activation of AMP-activated protein kinase (AMPK) (21). However, Scherer and colleagues (22) recently provided compelling evidence that adiponectin, by stimulating ceramidase activity, decreases intracellular

From the [1]Cellular and Molecular Metabolism Laboratory, Baker IDI Heart and Diabetes Institute, Melbourne, Victoria, Australia; the [2]Department of Physiology, Monash University, Clayton, Victoria, Australia; the [3]Lipidomics Laboratory, Baker IDI Heart and Diabetes Institute, Melbourne, Victoria, Australia; the [4]Department of Physiology, Kanazawa University, Kanazawa, Japan; and the [5]Molecular Signalling Laboratory, Centre for Cancer Biology, Adelaide, South Australia, Australia.

Corresponding author: Mark A. Febbraio, mark.febbraio@bakeridi.edu.au, or Clinton R. Bruce, clinton.bruce@monash.edu.

Received 9 January 2012 and accepted 21 June 2012.

DOI: 10.2337/db12-0029

This article contains Supplementary Data online at http://diabetes.diabetesjournals.org/lookup/suppl/doi:10.2337/db12-0029/-/DC1.

See accompanying commentary, p. 3081.

ceramide and concomitantly increases S1P. Hence, the dynamic balance between the levels of ceramide and S1P may have implications for the development of obesity-induced insulin resistance. The aim of the current study was, therefore, to examine the role of SphK in regulating skeletal muscle ceramide content and insulin sensitivity in conditions of lipid oversupply. We hypothesized that SphK1 overexpression would promote flux through the sphingolipid degradative pathway, which would prevent high-fat diet (HFD)–induced ceramide accumulation and, therefore, enhance muscle insulin action.

RESEARCH DESIGN AND METHODS

Animals. All experimental procedures were approved by the Alfred Medical Research and Education Precinct Animal Ethics Committee and were in accordance with the National Health and Medical Research Council (NHMRC) of Australia Guidelines on Animal Experimentation. Generation of the moderate-level or low-level SphK1a transgenic (SphK1 Tg) mice has been described elsewhere (23,24). Mice were maintained on a C57Bl/6 background (back-crossed ≥9 times). All experiments commenced when mice were 8 weeks old. Male SphK1 Tg mice and their wild-type (WT) littermates were kept in a temperature controlled room (22 ± 1°C) on a 12-h light/dark cycle with free access to food and water. Mice were fed a standard chow diet (14.3 MJ/kg, 76% of kJ from carbohydrate, 5% fat, 19% protein, Specialty Feeds, Glen Forrest, Western Australia, Australia). For the fat-feeding studies, mice were fed an HFD (19 MJ/kg, 35% of kJ from carbohydrate, 42% fat [42.7% saturated, 35.1 monounsaturated and 21.7% polyunsaturated FAs], 23% protein, Specialty Feeds) for 6 weeks. Lean and fat mass were determined using the EchoMRI 4-in-1 (Echo Medical Systems, Houston, TX).

Mice were randomly assigned to two groups that underwent procedures to determine *1*) skeletal muscle glucose uptake or *2*) activation of intracellular signaling molecules. Glucose tolerance tests were performed on a subset of mice from each group, and samples of plasma and tissue were collected for subsequent analysis. A separate group of WT and SphK1 Tg mice were fed an HFD and were studied under hyperinsulinemic clamp conditions (described below). The numbers for each group are presented in the table and figure legends.

Glucose tolerance tests. Intraperitoneal glucose tolerance tests (1 g/kg lean body mass) were performed on mice fasted for 5 h. Blood samples were obtained from the tail tip at the indicated times, and blood glucose levels were measured (AccuCheck II; Roche, Castle Hill, New South Wales, Australia).

In vivo electroporation. cDNA encoding the human *SphK2* gene was cloned into the pcDNA3.1 expression vector (25). Plasmids were injected into tibialis anterior muscles and electroporated by a previously described protocol (26,27). All experiments were performed 7 days after transfection.

Skeletal muscle incubations. Mice were fasted for 5 h and anesthetized by injection of sodium pentobarbitone (50 mg/kg i.p.). Glucose uptake in isolated extensor digitorum longus (EDL) muscle was assayed for 15 min using [^{3}H]-2-deoxy-D-glucose (1 mmol/L; 0.128 μCi/mL) as described previously (26). For analysis of insulin signaling, EDL muscles were incubated in Krebs-Henseleit buffer (pH 7.4), with or without insulin (300 μU/mL) for 30 min.

Hyperinsulinemic, euglycemic clamp. Mice were catheterized 4 days before hyperinsulinemic, euglycemic clamp studies. Mice were anesthetized with isoflurane (1–2% in oxygen), and the right jugular vein was catheterized with a Silastic catheter (0.025-inch outer diameter). The catheter was exteriorized at the back of the neck, filled with sterile saline, and sealed with a stainless steel plug. After surgery, animals were individually housed, and body weight was recorded daily. Hyperinsulinemic, euglycemic clamps were performed on 5-h fasted, conscious, restrained mice. The infusion protocol consisted of a 150-min tracer equilibration period (t = −150 to 0 min) beginning at 0830 h, followed by a 120-min experimental period (t = 0 to 120 min) beginning at 1000 h. A bolus of [3-^{3}H]glucose (5 μCi; PerkinElmer, Waltham, MA) was administered at t = −120 min, followed by a constant infusion of 0.05 μCi/min for 150 min. At t = −15 and −5 min, blood samples (~50 μL) were obtained from the tail tip for assessment of basal glucose, plasma insulin, and free FAs (FFAs), as well as glucose-specific activity. The hyperinsulinemic, euglycemic clamp was initiated at t = 0 min with an infusion of human insulin (4 mU · kg^{-1} · min^{-1}; ActRapid; Novo Nordisk, Baulkham Hills, New South Wales, Australia). To minimize changes in glucose specific activity, the [3-^{3}H]glucose infusion was increased to 0.1 μCi/min. Blood glucose was measured every 10 min, and euglycemia (~10–11 mmol/L) was maintained by infusing 30% dextrose as required. Blood samples (10 μL) were taken every 10 min from t = 80 to 120 min to determine glucose-specific activity. At 120 min, a bolus of 2[^{14}C]deoxyglucose ([^{14}C]2DG; 13 μCi; PerkinElmer, Waltham, MA) was administered via the catheter. Blood (10 μL) was taken at 2, 15, 25, and 35 min for the determination of [^{14}C]2DG. Mice were then anesthetized and tissues collected. Plasma insulin and FFA levels were determined from samples obtained from cardiac puncture on anesthetized mice at the end of the clamp procedure.

Determination of plasma and tissue radioactivity. Blood samples (10 μL) were deproteinized with barium hydroxide (0.3 N) and zinc sulfate (0.3 N), and [3-^{3}H]glucose and 2[^{14}C]DG radioactivity was determined by liquid scintillation counting. The rate of glucose appearance (endogenous R_a) and disappearance (R_d) were determined using steady-state equations. Endogenous glucose production during the clamp was calculated by subtracting the glucose infusion rate (GIR) from R_d. The insulin-stimulated component of the total R_d (IS-Rd) is equal to clamp R_d minus the basal glucose turnover rate. Accumulation of [^{14}C]2DG was determined in an aqueous extract of tissue after homogenization. Free and phosphorylated [^{14}C]2DG were separated by ion exchange chromatography on Dowex *l*-X8 columns (acetate form). The area under the tracer disappearance curve of [^{14}C]2DG, together with the radioactivity for the phosphorylated [^{14}C]2DG from individual tissues, were used to calculate the glucose metabolic index (Rg′) (28).

Western blotting. Tissues were lysed, and protein concentration was determined. Lysates were solubilized, 40 μg protein was loaded and resolved by SDS-PAGE on polyacrylamide gels, transferred to membranes, and blocked with 5% milk. Immunoblotting was performed using the following primary antibodies: phosphorylated (p)Akt serine 473 and total (t)Akt (Cell Signaling Technology, Danvers, MA), pJNK (Thr183/Tyr185) and tJNK (Cell Signaling Technology), as well as pIKK-β (Ser181), tIKK-β (Cell Signaling Technology). After incubation with appropriate secondary antibody, the immunoreactive proteins were detected with enhanced chemiluminescence and quantified by densitometry. Analysis of membrane and cytosolic protein kinase C θ (PKCθ) were performed as previously described (26).

Plasma analysis. Plasma insulin was measured by ELISA (Millipore, St. Louis, MO). FFAs were measured spectrophotometrically by an enzymatic colorimetric assay (NEFA C kit; Wako Chemicals, Richmond, VA). Plasma triglycerides were determined using a colorimetric assay kit (Triglycerides GPO-PAP; Roche Diagnostics, Indianapolis, IN). Plasma S1P concentration was assessed by S1P ELISA (Echelon, Salt Lake City, UT).

SphK activity and S1P. SphK activity in tissue homogenates was determined using D-*erythro*-sphingosine and [γ-^{32}P]ATP as substrates, as described previously (29). Muscle S1P levels were determined using previously described methods (30).

Lipid analysis. Lipids were extracted from plasma (10 μL) using a single-phase chloroform/methanol (2:1 v/v) extraction, as previously described (31) and were analyzed for ceramide content. For tissue lipids (DAG, ceramide, sphingomyelin, sphingosine, phosphatidylcholine [PC], and phosphatidylethanolamine [PE]), samples were homogenized in 300 μL 1xPBS (pH 7.47), and protein content was determined. Lipids were extracted from 50 μg protein for muscle, 10 μg protein for white adipose tissue (WAT) and 25 μg protein for liver. Lipids were extracted using a single-phase chloroform/methanol (2:1 v/v; 20 volumes) extraction after the addition of internal standards (100 pmol each of ceramide 17:0, PC 13:0/13:0, PE 17:0/17:0, sphingomyelin 12:0, and sphingosine 17:1; Avanti Polar Lipids, Alabaster, AL), together with 200 pmol DAG 15:0/15:0 (Sigma-Aldrich, St. Louis, MO). Samples were vortexed, mixed for 10 min, sonicated for 30 min, and left at room temperature for 20 min. Extracts were centrifuged at 13,000*g* for 10 min. The supernatant was transferred to a clean tube and dried under nitrogen at 40°C. Lipids were redissolved in 50 μL water-saturated butanol containing 10 mmol/L NH_4COOH, then 50 μL methanol containing 10 mmol/L NH_4COOH was added. Analysis was performed by electrospray ionization–tandem mass spectrometry using a PE Sciex API 4000 Q/TRAP mass spectrometer with a turbo-ionspray source and Analyst 1.5 data system, as described previously (32). Tissue TAG content was determined biochemically using a colorimetric assay kit (Triglycerides GPO-PAP; Roche Diagnostics).

RNA isolation and quantitative real-time RT-PCR. Total RNA was isolated from gastrocnemius muscle using Trizol (Invitrogen, Carlsbad, CA). Samples were reverse-transcribed using TaqMan reverse-transcription reagents (Applied Biosystems, Foster City, CA). Gene expression analysis was performed by RT-PCR using TaqMan gene expression assays (Applied Biosystems), including 18S and glyceraldehyde-3-phosphate dehydrogenase probe and primers for housekeeping measurements.

AMPK activity and markers of oxidative stress. AMPK activity was measured in tissue lysates as previously described (33). Malondialdehyde content was determined spectrophotometrically using BIOXTECH MDA-586 assay kit (Oxis Research, Portland, OR).

Statistics. Data are reported as mean ± SEM. Comparisons between data from multiple treatment groups were made using factorial ANOVA, followed by Newman-Keuls post hoc analysis. To specifically examine differences between WT and Tg mice, data were analyzed using the Mann-Whitney U test. Statistical significance was accepted at $P < 0.05$.

RESULTS

Muscle ceramide is reduced in SphK1 Tg mice. SphK1 Tg mice were indistinguishable from WT littermates with respect to body mass or fat mass (Table 1). We screened a number of metabolic tissues and only observed increased SphK activity in skeletal muscle (Fig. 1*A*). In addition, S1P levels tended to increase in muscle of SphK1 Tg mice relative to WT, but this was not statistically different (Fig. 1*B*). Furthermore, sphingosine content (Fig. 1*C*) was not altered, but the S1P-to-sphingosine ratio tended to be reduced in SphK1 Tg mice (0.61 ± 0.12) compared with WT mice (1.45 ± 0.16), although this was not statistically significant ($P > 0.05$). However, ceramide was reduced in the quadriceps and soleus, but not in WAT or liver (Fig. 1*D*). Despite these changes, when fed a chow diet, SphK1 Tg mice did not show any differences in fasting plasma glucose, insulin, FFAs, triglycerides, ceramides, or S1P compared with WT mice (Table 1). In addition, glucose tolerance was not different when compared with WT mice (Fig. 1*E*).

Because we only studied mice overexpressing SphK1, the possibility existed that SphK2 may play a role in metabolism. To our knowledge, a Tg mouse does not exist for SphK2, but to rule out the possibility that this isoform plays a role, we transiently overexpressed SphK2 in skeletal muscle using in vivo electroporation. SphK2 overexpression had no effect on intramuscular lipid content (Supplementary Fig. 1*A*–*C*), suggesting that SphK1, but not SphK2, plays a role in regulating muscle ceramide levels; therefore, further studies were focused entirely on SphK1.

SphK1 Tg mice are protected from HFD-induced ceramide accumulation. The HFD increased body mass and fat mass, as well as fasting plasma glucose, insulin, triglycerides, and S1P in both strains of mice, but there were no differences between SphK1 Tg and WT littermates (Table 1). In WT mice, the HFD increased total muscle ceramide by ~40% (445 ± 48 vs. 611 ± 50 pmol/mg protein for chow and HFD WT mice, respectively; $P < 0.05$; Fig. 2*A* and *B*). Importantly, however, this effect was ameliorated in SphK1 Tg mice (Fig. 2*A*) to an extent where muscle from these mice was resistant to the effects of the HFD with respect to ceramide accumulation (Fig. 2*B*). Despite these effects, neither fat-feeding nor SphK1 overexpression affected the expression of acid ceramidase (Supplementary Fig. 6). Similar to our findings in chow-fed mice, muscle S1P and sphingosine were not altered in SphK1 Tg relative to WT mice (Fig. 2*C* and *D*).

Consistent with a reduction in ceramide, overexpression of SphK1 resulted in a reduction in C18:0 sphingomyelin (Supplementary Fig. 2*A*), the most predominant species in muscle, and in total sphingomyelin levels (Fig. 2*E*). In addition, a number of sphingomyelin species were increased in response to the HFD (Supplementary Fig. 2*A*). The HFD also increased muscle DAG (Fig. 2*F* and Supplementary Fig. 2*B*) and TAG (Fig. 2*G*), which was independent of the genetic strain of mice. Interestingly, despite the increase in DAG with an HFD, the membrane-to-cytosol ratio of PKCθ was not altered (Supplementary Fig. 3). Although S1P can be hydrolyzed by S1P lyase to form hexadecanol and phosphoethanolamine, of which the later can be used for the biosynthesis of PE, S1P lyase expression and activity in skeletal muscle is almost undetectable (34); thus, the relevance of this pathway in muscle is questionable. Nonetheless, we analyzed muscle PE content to determine whether SphK1 overexpression altered this lipid. In addition, it has recently been suggested that the ratio between PC and PE is altered as a consequence of obesity, resulting in cellular stress (35). Therefore, we also analyzed the PC content. However, in this model, neither diet nor SphK1 overexpression affected PE (Fig. 2*H*) or PC (Fig. 2*H*) levels in muscle.

HFD-induced muscle insulin resistance is ameliorated in SphK1 Tg mice. Because HFD-induced increase in muscle ceramide accumulation was prevented in SphK1 Tg mice, we examined whether these mice would have improved glucose homeostasis. Initial studies showed that glucose tolerance was improved in SphK1 Tg mice fed an HFD compared with WT mice (Fig. 3*A*). Ex vivo glucose uptake assays revealed no differences in chow-fed WT or SphK1 Tg mice; however, consistent with our glucose tolerance data, insulin-stimulated glucose uptake was enhanced in HFD SphK1 Tg mice compared with HFD WT mice (Supplementary Fig. 4*A* and *B*). Although insulin sensitivity was improved in HFD SphK1 Tg mice, it was not restored to those levels observed in chow-fed mice (Supplementary Fig. 3*A* and *B*).

Given these observations, we performed hyperinsulinemic, euglycemic clamp studies in SphK1 Tg and WT mice fed the HFD. Glucose levels were successfully clamped at basal levels in both strains (Fig. 3*B*), and no differences were observed in plasma insulin or FFA levels during the clamp (Table 1). Basal rates of glucose production were not different between strains (Fig. 3*D*). The GIR during the

TABLE 1
Characteristics of chow- and HFD-fed WT and SphK1 Tg mice

	Chow				HFD			
	WT	*n*	SphK1 Tg	*n*	WT	*n*	SphK1 Tg	*n*
Body mass (g)*	30.4 ± 0.9	15	31.0 ± 1.1	10	37.0 ± 0.9	22	36.8 ± 1.1	17
Fat mass (g)*	3.2 ± 0.4	15	3.0 ± 0.6	10	10.8 ± 0.7	22	11.2 ± 0.8	17
Fasting blood glucose (mmol/L)*	9.6 ± 0.4	15	10.5 ± 0.3	10	12.2 ± 0.5	15	11.9 ± 0.6	13
Fasting plasma insulin (ng/mL)*	0.50 ± 0.05	7	0.47 ± 0.04	8	2.48 ± 0.34	14	2.23 ± 0.31	8
15-min IPGTT plasma insulin (ng/mL)	0.77 ± 0.13†	7	1.22 ± 0.14†	8	2.75 ± 0.37	14	2.21 ± 0.35	8
Clamp plasma insulin (ng/mL)	ND		ND		6.55 ± 0.83	5	5.41 ± 0.76	6
Fasting plasma FFA (mmol/L)	0.59 ± 0.10	12	0.70 ± 0.12	9	0.66 ± 0.06	5	0.61 ± 0.03	6
Clamp plasma FFA (mmol/L)	ND		ND		0.44 ± 0.07	5	0.40 ± 0.02	6
Fasting plasma triglyceride (mmol/L)*	0.35 ± 0.03	8	0.42 ± 0.05	5	0.50 ± 0.04	10	0.58 ± 0.05	10
Fasting plasma ceramide (μmol/L)	1.99 ± 0.28	13	2.34 ± 0.41	10	2.59 ± 0.19	19	2.60 ± 0.16	16
Fasting plasma S1P (μmol/L)*	0.20 ± 0.08	6	0.10 ± 0.06	4	0.47 ± 0.06	5	0.52 ± 0.05	5

Data are mean ± SEM. IPGTT, intraperitoneal glucose tolerance test; ND, not determined. *$P < 0.05$ main effect for diet; †$P < 0.05$ vs. fasting.

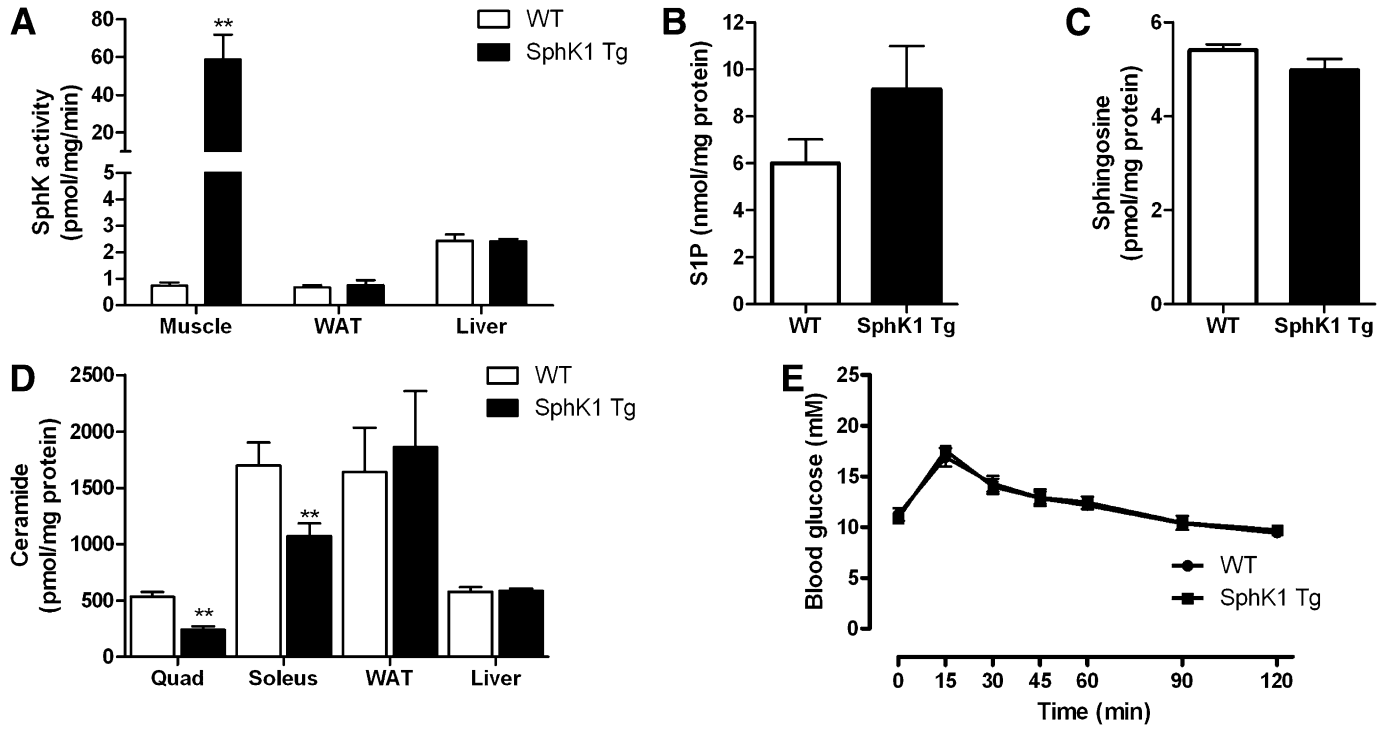

FIG. 1. Phenotypic data from chow-fed WT and SphK1 Tg mice. *A*: SphK1 activity in muscle, WAT, and liver (WT n = 8; SphK1 Tg n = 5). *B*: Muscle S1P content (WT n = 7; SphK1 Tg n = 6). *C*: Muscle sphingosine content (WT n = 7; SphK1 Tg n = 6). *D*: Ceramide levels in quadriceps (Quad) (WT n = 7; SphK1 Tg n = 5), soleus (WT n = 7; SphK1 Tg n = 6), WAT (WT n = 10; SphK1 Tg n = 10), and liver (WT n = 8; SphK1 Tg n = 5). *E*: Glucose tolerance curves (WT n = 15; SphK1 Tg n = 10). Data are mean ± SEM. **$P < 0.01$ vs. WT.

clamp was markedly higher in SphK1 Tg compared with WT mice (Fig. 3*C*). This was primarily due to improved muscle insulin sensitivity because IS-Rd was higher in SphK1 Tg compared with WT mice (Fig. 3*E*). In contrast, the suppression of hepatic glucose production during the clamp was comparable between SpK1 Tg and WT mice (Fig. 3*F*), indicating that hepatic insulin action was not affected by SphK1 overexpression in muscle. This was expected because the HFD-induced increase in liver lipids (Supplementary Fig. 5*A*–*C*) was not different when comparing SphK1 Tg with WT mice. Tissue-specific glucose uptake (Rg′) during the clamp was augmented in hind limb muscle from SphK1 Tg mice (EDL, tibialis anterior, and quadriceps), but not in WAT (Fig. 3*G*). We also examined the effect of SphK1 overexpression on Akt phosphorylation in isolated EDL muscles. Insulin-stimulated Akt phosphorylation was increased in HFD SphK1 Tg mice compared with HFD WT mice (Fig. 3*H*–*J*).

SphK1 Tg mice are protected from HFD-induced JNK activation. The phosphorylation of IKK-β was neither affected by diet nor genotype (Fig. 4*A*). In contrast, the HFD induced a significant increase in JNK phosphorylation, but this was attenuated in SphK1 Tg mice (Fig. 4*B*). We also examined whether proinflammatory cytokines or markers of macrophage infiltration were affected by diet or mouse genetic strain in skeletal muscle. Although *F4/80* mRNA was increased by the HFD, no such effect was seen for interleukin 6 or tumor necrosis factor-α expression. The expression of these genes was unaffected by SphK1 overexpression, irrespective of diet (Supplementary Fig. 6). To confirm the in vivo results, we used an alternative model system, high concentrations of the saturated FA palmitate, to activate JNK in muscle. Isolated soleus muscles from WT and SphK1 Tg mice were incubated in the presence of low-dose (control; 0.5 mmol/L) and high-dose (2.0 mmol/L) palmitate. Incubation of high-dose palmitate uniformly increased the accumulation of ceramide species, as well as total ceramide, but this increase was blunted when the skeletal muscle of SphK1 Tg was compared with WT mice (Fig. 4*C*). In this model, the palmitate-induced phosphorylation of JNK was also markedly attenuated in muscle from SphK1 Tg mice (Fig. 4*D*).

Overexpression of SphK1 does not alter markers of angiogenesis, oxidative stress, or AMPK activity. Because Sphk1/S1P has been implicated in regulating angiogenesis (23), oxidative stress (24), and AMPK activity (36), it is possible that any one of these factors could be affected by SphK1 overexpression and influence muscle insulin sensitivity. Therefore, the expression of numerous markers of angiogenesis was determined, including cluster of differentiation (CD) 31, platelet-derived growth factor (PDGF), and vascular endothelial growth factor (VEGF). The expression of *CD31* was unaffected by diet or genotype, whereas *PDGF* was reduced with the HFD, and *VEGF* expression was lower in muscle of SphK1 Tg mice (Supplementary Fig. 6). The content of malondialdehyde, a marker of tissue oxidative stress, was not altered by the HFD or SphK1 overexpression (Supplementary Fig. 7*A*). Furthermore, muscle AMPK activity was similar in all groups studied (Supplementary Fig. 7*B*).

DISCUSSION

Ceramide is a potent lipid-signaling molecule that can cause insulin resistance by impairing activation of the insulin-signaling pathway. Moreover, preventing ceramide accumulation by inhibiting de novo ceramide synthesis protects against insulin resistance (9,10). It is well known

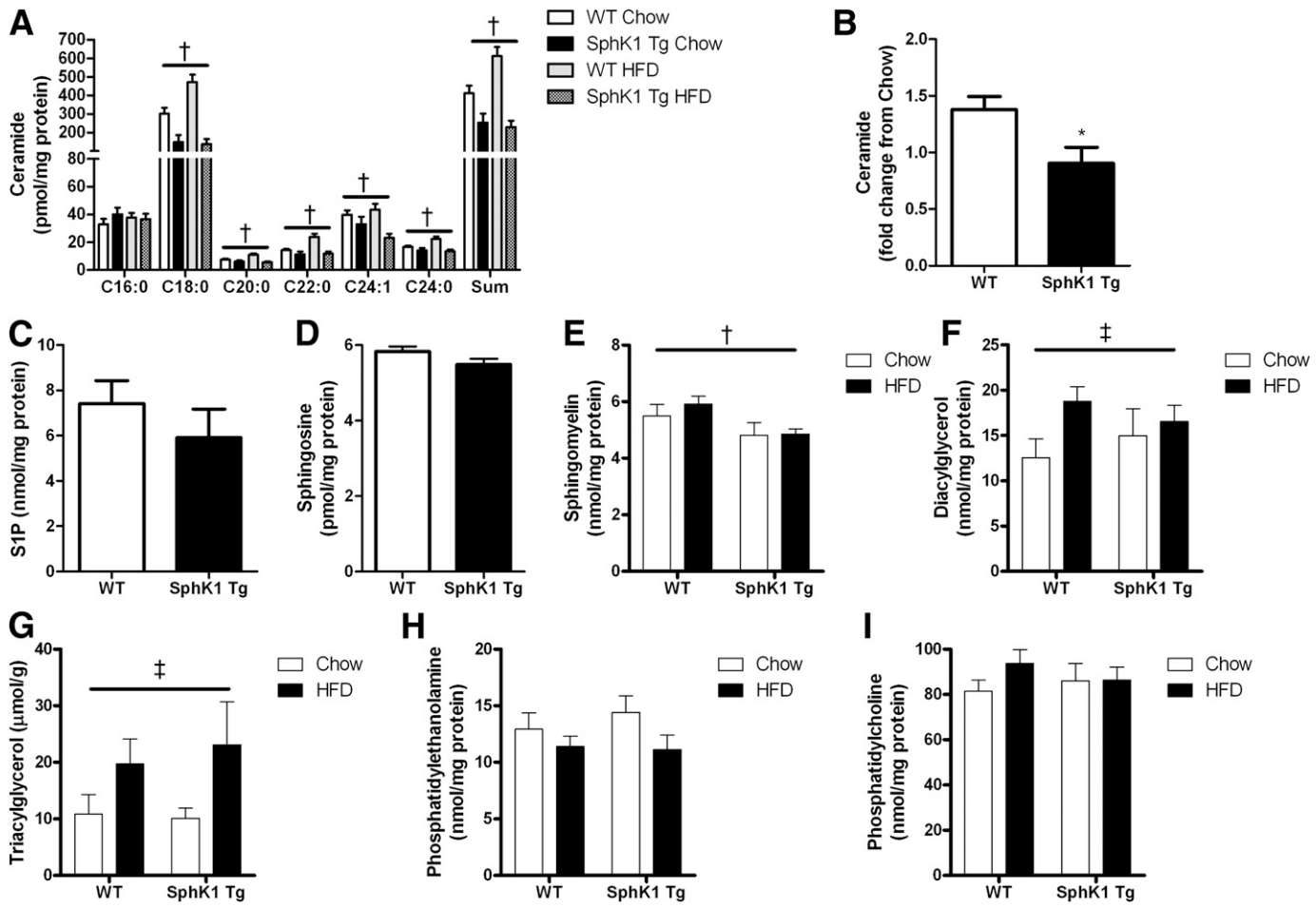

FIG. 2. Muscle lipid levels in chow-fed and HFD-fed WT and SphK1 Tg mice. *A*: Ceramide levels (chow WT $n = 7$; chow SphK1 Tg $n = 5$; HFD WT $n = 15$; HFD SphK1 Tg $n = 15$). *B*: Fold change in total ceramide content (data expressed relative to chow group of the same genotype; $n = 15$). *C*: S1P content in muscle of HFD-fed WT ($n = 8$) and SphK1 Tg mice ($n = 7$). *D*: Muscle sphingosine content (WT $n = 8$; SphK1 Tg $n = 7$). *E*: Muscle sphingomyelin levels (chow WT $n = 5$; chow SphK1 Tg $n = 5$; HFD WT $n = 7$; HFD SphK1 Tg $n = 7$). *F*: Muscle DAG profile (chow WT $n = 5$; chow SphK1 Tg $n = 5$; HFD WT $n = 7$; HFD SphK1 Tg $n = 7$). *G*: Muscle TAG content (chow WT $n = 6$; chow SphK1 Tg $n = 7$; HFD WT $n = 10$; HFD SphK1 Tg $n = 8$). *H*: PE levels (chow WT $n = 5$; chow SphK1 Tg $n = 5$; HFD WT $n = 7$; HFD SphK1 Tg $n = 7$). *I*: PC levels (chow WT $n = 5$; chow SphK1 Tg $n = 5$; HFD WT $n = 7$; HFD SphK1 Tg $n = 7$). Data are mean ± SEM. *$P < 0.05$ vs. wild type. †Main effect for genotype, $P < 0.05$. ‡Main effect for diet, $P < 0.05$.

that SphK1 prevents ceramide accumulation by promoting its metabolism into S1P, but to date, the role of SphK1 in the etiology of obesity and insulin resistance has not been directly examined. Here, we provide novel evidence that SphK1 is an important enzyme that regulates ceramide metabolism and insulin sensitivity in skeletal muscle. These findings highlight that in addition to inhibiting ceramide synthesis, targeting pathways to enhance ceramide degradation may be beneficial in treating muscle insulin resistance.

Several hypotheses have been proposed to define the molecular pathways that impair insulin action. Insulin resistance is associated with ectopic lipid deposition in liver and muscle (2); moreover, the accumulation of deleterious lipids, such as DAG (5) and ceramide (10), dysregulate insulin action directly (6) or indirectly via the activation of serine threonine kinases such JNK (7). Data from the current study, at least with respect to SphK1 overexpression, suggest that ceramide accumulation and JNK activation in muscle are involved in HFD-induced insulin resistance in mice. When SphK1 Tg mice were fed the HFD, ceramide levels were not increased above those observed in chow-fed Tg animals. These results were accompanied by improved whole-body and skeletal muscle insulin sensitivity (Fig. 3*A–F* and Supplementary Fig. 4), improved insulin-stimulated Akt phosphorylation (Fig. 3*G–I*), and an attenuated JNK phosphorylation in muscle (Fig. 4). Together, these data suggest that overexpression of SphK1 in skeletal muscle prevents ceramide accumulation and bioactivity, which improves insulin action, in part, by improving insulin signaling and preventing JNK phosphorylation.

Overexpression of SphK1 may be expected to increase S1P levels. In the current study, we did not detect an increase in intramuscular S1P content in SphK1 Tg mice (Fig. 1*B*, Fig. 2*C*). Although somewhat unexpected, these findings are similar to those of Takuwa et al. (24), who found that tissue S1P was only modestly increased in SphK1 Tg mice with high-level overexpression, whereas in mice with low-level overexpression, S1P was not different to WT mice. This suggests that any increase in S1P production caused by overexpressing SphK1 is balanced by S1P breakdown (23). Nonetheless, these findings have important implications for the current study because they suggest that SphK1 overexpression in these circumstances improves metabolic homeostasis by reducing ceramide accumulation per se and not via any effect due to an increase in intracellular S1P.

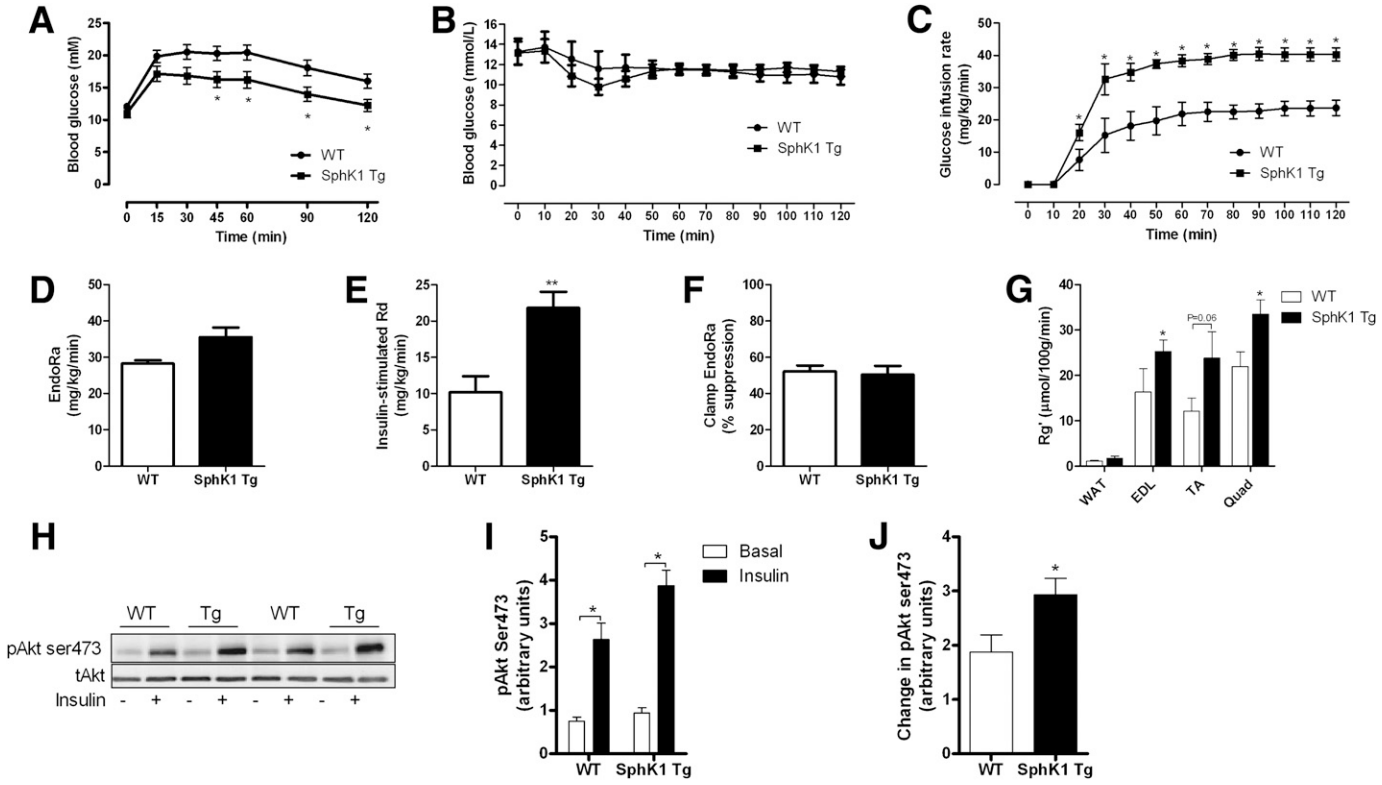

FIG. 3. Glucose tolerance and insulin sensitivity is enhanced in SphK1 Tg mice fed an HFD. *A*: Blood glucose levels during a glucose tolerance test in HFD-fed WT (n = 22) and SphK1 Tg (n = 17) mice. *B*: Blood glucose levels during the hyperinsulinemic, euglycemic clamp (WT n = 5; SphK1 Tg n = 6). *C*: Glucose infusion rate (WT n = 5; SphK1 Tg n = 6). *D*: Basal rates of endogenous glucose R_a (EndoRa) (WT n = 5; SphK1 Tg n = 6). *E*: Insulin-stimulated glucose R_d (WT n = 5; SphK1 Tg n = 6). *F*: Percent suppression of EndoRa (WT n = 5; SphK1 Tg n = 6). *G*: Tissue glucose uptake (WT n = 5; SphK1 Tg n = 6). *H*: Immunoblot of pAkt serine (ser) 473 in basal and insulin-stimulated EDL muscles ex vivo (n = 8 for each group). *I*: Quantification of pAkt ser473 (n = 8 for each group). *J*: Fold change in pAkt ser473 under insulin-stimulated conditions. Data are mean ± SEM; n = 17–22 for the glucose tolerance data (n = 8 for each group). *P < 0.05 vs. WT; **P < 0.01 vs. WT. TA, tibialis anterior; Quad, quadriceps.

Although our study reveals an important role for SphK1 in regulating muscle ceramide, we cannot discount the possibility that overexpression of SphK1 altered the activity of other enzymes involved in sphingolipid metabolism. In this regard, sphingomyelin levels were lower in muscle from SphK1 Tg mice. However, rather than being mediated by alterations in enzyme activity, this effect may simply be driven by the reduction in ceramide itself. In support of such a precursor relationship is the fact that the C18:0 species of both ceramide and sphingomyelin were reduced by SphK1 overexpression. Nonetheless, because sphingolipid enzymes, such as serine palmitoyltransferase, ceramidase, and sphingomyelinase, are regulated by factors such as exercise training (37) and HFD (38), it is possible that the activity of these enzymes was altered in SphK1 Tg mice, which may, in part, contribute to the observed effects on muscle ceramide metabolism.

Previous studies have implicated SphK1 in playing a role in regulating muscle blood flow and angiogenesis (23), factors that could alter muscle insulin sensitivity. Our data showing enhanced insulin-stimulated glucose uptake ex vivo (Supplementary Fig. 4) suggests that the effects of SphK1 overexpression on muscle insulin sensitivity are independent of changes in blood flow and angiogenesis. In this ex vivo system, differences in muscle capillarization and blood flow are circumvented as substrate delivery occurs via diffusion from the incubation medium. Furthermore, we determined the expression of a number of markers of angiogenesis in muscle. Although *CD31* expression was unaffected by diet or genotype, *PDGF* was reduced with the HFD and *VEGF* was lower in muscle of SphK1 Tg mice. Taken together, these data do not support a role for increased angiogenesis or blood flow contributing to the improvement in insulin action in the HFD SphK1 Tg mice.

In addition to ceramide, DAG accumulation is associated with muscle insulin resistance (4,5). Overexpression of SphK1 reduced ceramide levels, but the HFD-induced increase in DAG was unaffected. Interestingly, the improvement in insulin-stimulated glucose uptake in HFD SphK1 Tg mice was not sufficient to restore insulin sensitivity to chow-fed levels (Supplementary Fig. 4). Thus, it is possible that DAG mediated the residual insulin resistance in fat-fed SphK1 Tg mice. Although the mechanism by which DAG causes insulin resistance is not completely understood, it is possible that activation of PKC isoforms is involved. We have previously shown that fat-feeding in rats increases muscle DAG and leads to an increase in the membrane-to-cytosol ratio of PKCθ (27) and that preventing DAG accumulation by increasing FA oxidation blocks the redistribution of PKCθ to the membrane; however, we did not detect any differences in the localization of PKCθ in the current study. These findings suggest that other PKC isoforms not analyzed, such as PKCδ and PKCε, may play a role in DAG-mediated insulin resistance or implicate PKC-independent mechanisms. Regardless, our data indicate that ceramide and DAG are both likely to contribute to the development of insulin resistance in muscle.

In summary, our data reveal that SphK1 is a key enzyme that reduces the accumulation of muscle ceramide in

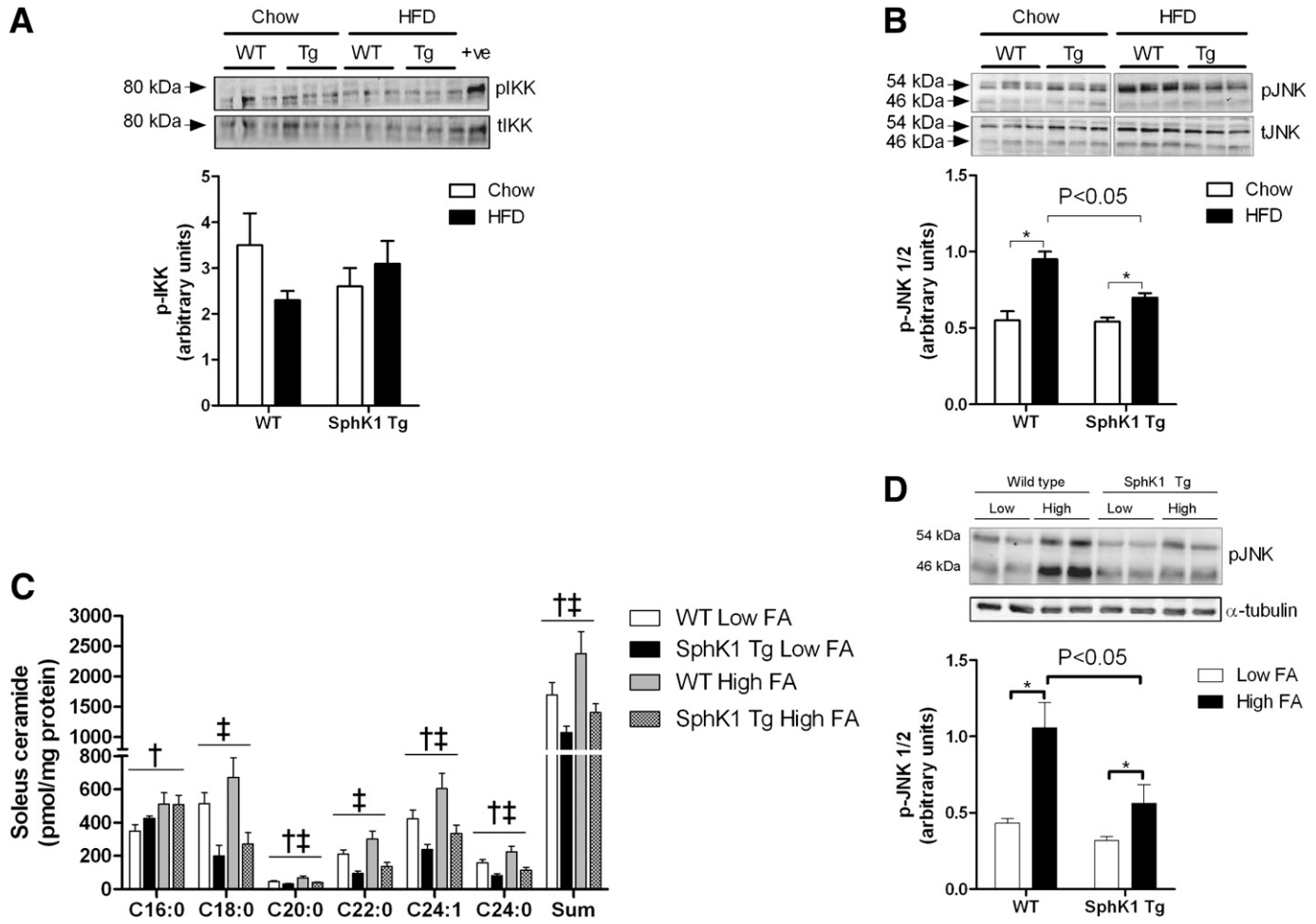

FIG. 4. Inflammatory markers in skeletal muscle of WT and SphK1 Tg mice. *A*: pIKK in muscle from chow- and HFD-fed mice (chow WT $n = 7$; chow SphK1 Tg $n = 5$; HFD WT $n = 9$; HFD SphK1 Tg $n = 10$). *B*: pJNK in muscle from chow- and HFD-fed mice (chow WT $n = 7$; chow SphK1 Tg $n = 5$; HFD WT $n = 9$; HFD SphK1 Tg $n = 10$). *C*: Ceramide profile of soleus muscles incubated with low (0.5 mmol/L; $n = 8$ for WT; $n = 6$ for SphK1 Tg) and high (2.0 mmol/L; $n = 10$ for WT; $n = 8$ for SphK1 Tg) palmitate for 6 h. *D*: pJNK in soleus muscles incubated with low (0.5 mmol/L) and high (2.0 mmol/L) palmitate for 6 h ($n = 12$ for each group). Data are mean ± SEM. For *B* and *D*: *$P < 0.05$ for specified comparisons. For *C*: †$P < 0.05$ main effect for palmitate; ‡$P < 0.05$ main effect for genotype.

conditions of lipid oversupply. This is important because ceramide has previously been shown to activate JNK and inhibit insulin signaling, which both contribute to decreased insulin action. These data identify SphK1 as an important regulator of lipid partitioning in skeletal muscle, thereby highlighting the potential for targeting pathways to enhance ceramide degradation for the prevention and/or treatment of obesity-induced muscle insulin resistance.

ACKNOWLEDGMENTS

This work was supported by NHMRC Project Grant 526608 to C.R.B. and the Victorian Government Operational Infrastructure Support Program. C.R.B. is a Career Development Fellow. S.M.P. and P.J.M. are Senior Research Fellows, and M.A.F. is a Senior Principal Research Fellow of the NHMRC.

No potential conflicts of interest relevant to this article were reported.

C.R.B. and M.A.F. designed the research, wrote the manuscript, and contributed to the writing of the final submitted version of the manuscript. S.R., J.R.B., C.Y., G.M.K., A.S., R.S.L.-Y., and J.M.W. performed research and contributed to the writing of the final submitted version of the manuscript. K.Y., Y.T., and P.J.M. contributed new reagents and analytical tools and contributed to the writing of the final submitted version of the manuscript. S.M.P. designed the research, contributed new reagents and analytical tools, and contributed to the writing of the final submitted version of the manuscript. M.A.F. and C.R.B. are the guarantors of this work and, as such, had full access to all the data in the study and take responsibility for the integrity of the data and the accuracy of the data analysis.

REFERENCES

1. Schenk S, Saberi M, Olefsky JM. Insulin sensitivity: modulation by nutrients and inflammation. J Clin Invest 2008;118:2992–3002
2. Savage DB, Petersen KF, Shulman GI. Disordered lipid metabolism and the pathogenesis of insulin resistance. Physiol Rev 2007;87:507–520
3. Holland WL, Knotts TA, Chavez JA, Wang LP, Hoehn KL, Summers SA. Lipid mediators of insulin resistance. Nutr Rev 2007;65:S39–S46
4. Itani SI, Ruderman NB, Schmieder F, Boden G. Lipid-induced insulin resistance in human muscle is associated with changes in diacylglycerol, protein kinase C, and IkappaB-alpha. Diabetes 2002;51:2005–2011
5. Chibalin AV, Leng Y, Vieira E, et al. Downregulation of diacylglycerol kinase delta contributes to hyperglycemia-induced insulin resistance. Cell 2008;132:375–386

6. Schmitz-Peiffer C, Craig DL, Biden TJ. Ceramide generation is sufficient to account for the inhibition of the insulin-stimulated PKB pathway in C2C12 skeletal muscle cells pretreated with palmitate. J Biol Chem 1999;274:24202–24210
7. Verheij M, Bose R, Lin XH, et al. Requirement for ceramide-initiated SAPK/JNK signalling in stress-induced apoptosis. Nature 1996;380:75–79
8. Hirosumi J, Tuncman G, Chang L, et al. A central role for JNK in obesity and insulin resistance. Nature 2002;420:333–336
9. Holland WL, Bikman BT, Wang LP, et al. Lipid-induced insulin resistance mediated by the proinflammatory receptor TLR4 requires saturated fatty acid-induced ceramide biosynthesis in mice. J Clin Invest 2011;121:1858–1870
10. Holland WL, Brozinick JT, Wang LP, et al. Inhibition of ceramide synthesis ameliorates glucocorticoid-, saturated-fat-, and obesity-induced insulin resistance. Cell Metab 2007;5:167–179
11. Hannun YA, Obeid LM. Principles of bioactive lipid signalling: lessons from sphingolipids. Nat Rev Mol Cell Biol 2008;9:139–150
12. Maceyka M, Sankala H, Hait NC, et al. SphK1 and SphK2, sphingosine kinase isoenzymes with opposing functions in sphingolipid metabolism. J Biol Chem 2005;280:37118–37129
13. Edsall LC, Cuvillier O, Twitty S, Spiegel S, Milstien S. Sphingosine kinase expression regulates apoptosis and caspase activation in PC12 cells. J Neurochem 2001;76:1573–1584
14. Spiegel S, Milstien S. The outs and the ins of sphingosine-1-phosphate in immunity. Nat Rev Immunol 2011;11:403–415
15. Di A, Kawamura T, Gao XP, et al. A novel function of sphingosine kinase 1 suppression of JNK activity in preventing inflammation and injury. J Biol Chem 2010;285:15848–15857
16. Hotamisligil GS. Inflammation and metabolic disorders. Nature 2006;444:860–867
17. Kapitonov D, Allegood JC, Mitchell C, et al. Targeting sphingosine kinase 1 inhibits Akt signaling, induces apoptosis, and suppresses growth of human glioblastoma cells and xenografts. Cancer Res 2009;69:6915–6923
18. Cuvillier O, Pirianov G, Kleuser B, et al. Suppression of ceramide-mediated programmed cell death by sphingosine-1-phosphate. Nature 1996;381:800–803
19. Takabe K, Paugh SW, Milstien S, Spiegel S. "Inside-out" signaling of sphingosine-1-phosphate: therapeutic targets. Pharmacol Rev 2008;60:181–195
20. Lancaster GI, Febbraio MA. Adiponectin sphings into action. Nat Med 2011;17:37–38
21. Yamauchi T, Kamon J, Minokoshi Y, et al. Adiponectin stimulates glucose utilization and fatty-acid oxidation by activating AMP-activated protein kinase. Nat Med 2002;8:1288–1295
22. Holland WL, Miller RA, Wang ZV, et al. Receptor-mediated activation of ceramidase activity initiates the pleiotropic actions of adiponectin. Nat Med 2011;17:55–63
23. Oyama O, Sugimoto N, Qi X, et al. The lysophospholipid mediator sphingosine-1-phosphate promotes angiogenesis in vivo in ischaemic hindlimbs of mice. Cardiovasc Res 2008;78:301–307
24. Takuwa N, Ohkura S, Takashima S, et al. S1P3-mediated cardiac fibrosis in sphingosine kinase 1 transgenic mice involves reactive oxygen species. Cardiovasc Res 2010;85:484–493
25. Pitson SM, D'andrea RJ, Vandeleur L, et al. Human sphingosine kinase: purification, molecular cloning and characterization of the native and recombinant enzymes. Biochem J 2000;350:429–441
26. Bruce CR, Brolin C, Turner N, et al. Overexpression of carnitine palmitoyltransferase I in skeletal muscle in vivo increases fatty acid oxidation and reduces triacylglycerol esterification. Am J Physiol Endocrinol Metab 2007;292:E1231–E1237
27. Bruce CR, Hoy AJ, Turner N, et al. Overexpression of carnitine palmitoyltransferase-1 in skeletal muscle is sufficient to enhance fatty acid oxidation and improve high-fat diet-induced insulin resistance. Diabetes 2009;58:550–558
28. Kraegen EW, James DE, Jenkins AB, Chisholm DJ. Dose-response curves for in vivo insulin sensitivity in individual tissues in rats. Am J Physiol 1985;248:E353–E362
29. Pitson SM, Moretti PA, Zebol JR, et al. Activation of sphingosine kinase 1 by ERK1/2-mediated phosphorylation. EMBO J 2003;22:5491–5500
30. Leclercq TM, Moretti PA, Vadas MA, Pitson SM. Eukaryotic elongation factor 1A interacts with sphingosine kinase and directly enhances its catalytic activity. J Biol Chem 2008;283:9606–9614
31. Meikle PJ, Wong G, Tsorotes D, et al. Plasma lipidomic analysis of stable and unstable coronary artery disease. Arterioscler Thromb Vasc Biol 2011;31:2723–2732
32. Matthews VB, Allen TL, Risis S, et al. Interleukin-6-deficient mice develop hepatic inflammation and systemic insulin resistance. Diabetologia 2010;53:2431–2441
33. Lee-Young RS, Griffee SR, Lynes SE, et al. Skeletal muscle AMP-activated protein kinase is essential for the metabolic response to exercise in vivo. J Biol Chem 2009;284:23925–23934
34. Ikeda M, Kihara A, Igarashi Y. Sphingosine-1-phosphate lyase SPL is an endoplasmic reticulum-resident, integral membrane protein with the pyridoxal 5′-phosphate binding domain exposed to the cytosol. Biochem Biophys Res Commun 2004;325:338–343
35. Fu S, Yang L, Li P, et al. Aberrant lipid metabolism disrupts calcium homeostasis causing liver endoplasmic reticulum stress in obesity. Nature 2011;473:528–531
36. Levine YC, Li GK, Michel T. Agonist-modulated regulation of AMP-activated protein kinase (AMPK) in endothelial cells. Evidence for an AMPK -> Rac1 -> Akt -> endothelial nitric-oxide synthase pathway. J Biol Chem 2007;282:20351–20364
37. Błachnio-Zabielska A, Zabielski P, Baranowski M, Gorski J. Aerobic training in rats increases skeletal muscle sphingomyelinase and serine palmitoyltransferase activity, while decreasing ceramidase activity. Lipids 2011;46:229–238
38. Zabielski P, Baranowski M, Błachnio-Zabielska A, Zendzian-Piotrowska M, Górski J. The effect of high-fat diet on the sphingolipid pathway of signal transduction in regenerating rat liver. Prostaglandins Other Lipid Mediat 2010;93:75–83